Noise and Texture Detection in Image Processing

Svetlana Roudenko *

May 25, 2004

Abstract

The idea of decomposing a given image into the cartoon part and the texture-noise part has become classical and there are basic standard algorithms to do that such as Rudin-Osher-Fatemi [ROF92], and modifications (e.g. Meyer [Mey01]; Osher, Solé, Vese [OSV03] and others). We discuss the Osher-Solé-Vese $\dot{H}^{-1}$-model of image decomposition and propose several natural modifications by using alternative flows aimed at faster and better decomposition of the image into the cartoon part and the texture-noise part.

Contents

1 Introduction

One of the main objectives in image processing is noise and texture detection. Given an image, its goal is to produce a more usfule image according to a given criteria. In many applications, the measured image is polluted by noise or blur. The distorted image has to be denoised in order to understnad the essential parts of the image. If one can understand how to separate noise and texture form in the given image, then the task of the denoising will be accomplished by removing the appropriate parts.

There are numerous approaches to image restoration in the literature: spacetral (or Fourier) methods, wavelets transform methods, statistical approaches (Wiener filtering), least square algorithms. Recently, a new class of methods has been interoduced: algorithms based on non-linear partial differential equations which use the total variation (TV) minimization technique. The last approach is of a special interest in this paper and we discuss alternative decompositions.

*This work was partially done under the contract W-7405-ENG-36 funded by Los Alamos National Lab

Before we discuss our model, we mention wavelet methods. Wavelet Analysis has been a new area of research which grew out of discovering the compactly supported wavelets (e.g., see [D92]) and has found a lot of applications in industry and engineering. For noise detection and image restoration there are basic thresholding techniques (soft, hard. wavelet shrinkage, e.g., see [DJ94], [DJKP96], [DJKP97]) which overall produce a good image recovery but have significant limitations beyond which methods can not be improved. In this research the author found that the TV minimization technique as described below gives much better results in texture and noise decompositions.

The large class of imaging models consists of decomposing a signal f, into two components: u and v. The first component, u, is aimed at modeling the objects which are present in a given image, that is, the cartoon part of f, while the second term, v, is responsible for the texture and noise present in the image. There are three main models of $u+v$ representation of an image f:

- the Osher-Rudin model (see [RO94], [ROF92]) which is the most common in image analysis;
- the Mamford-Shah model (refer to [MS85])
- and the DeVore-Lucier model [DL92].

In this project we consider the first model.

The TV model of image decomposition, introduced by Rudin, Osher and Fatemi [ROF92], [RO94] is described by the functional

$$E_{ROF}(u) = \|u\|_{BV} + \lambda \|f-u\|_{L^2}^2.$$

In this model, the decomposition of the image f (into the cartoon part u and the texture-noise part $v = f-u$) is done by minimizing the value of the functional $E(u)$.

The model of image decomposition proposed by Meyer [Mey01] is described by the functional

$$E_{Meyer}(u) = \|u\|_{BV} + \lambda \|f-u\|_{G}.$$

This model has an important advantage over the standard TV model: as Meyer shows in [Mey01], the texture and the noise have very small norms in the space G, so the model is better at extracting them from the image. On the other hand, an implicit nature of the norm in the G-space poses serious computational challenges for using the Meyer model in image processing. Let us remind that this norm is defined by

$$\|f\|_* \equiv \|f\|_G \equiv \inf_{\boldsymbol{g}:\ f=\nabla\cdot\boldsymbol{g}} \| \, |\boldsymbol{g}| \, \|_{L^\infty(\mathbb{R}^n)}, \qquad \text{where} \quad \boldsymbol{g} \in L^\infty(\mathbb{R}^n, \mathbb{R}^n) \quad \text{vanishes weakly at infinity.}$$

Attempts to modify the Meyer model led to several alternative $u+v$ and $u+v+w$ models; see, for example, [VO03, OSV03] (and other reports by the Applied Math group at UCLA). We are particularly interested in the Osher-Solé-Vese $\dot{H}^{-1}$-model

$$E_{OSV}(u) = \|u\|_{BV} + \lambda \|f-u\|_{\dot{H}^{-1}}^2, \tag{1.1}$$

introduced in [OSV03], which seems to be very good at extracting the texture and the noise. The sample pictures in [OSV03] show that the u-part in the Osher-Solé-Vese model gives sharper picture than in the standard TV model, while the texture-noise part v does not contain any

regular patterns of the original image f, only representing seemingly chaotic patterns (as opposed to "shades" still present in the v-part of the TV model).

We will explore the Osher-Solé-Vese model, aiming at faster and better decomposition of the image f into the cartoon and texture-noise parts.

In the next section we give a brief overview of the Osher-Solé-Vese model. In section 3 we suggest alternative flows. In section 4 we make a remark with numerical calculations on independence of the Osher-Solé-Vese model on the second term in the $u+v$ decomposition. In the last section (section 5), we discuss how to make sense of the second term and in which space its norm should be measured. That last section includes most of the numerical calculations.

2 The Osher-Solé-Vese model

We consider the $\dot{H}^{-1}$-model proposed by Osher, Solé, and Vese in [OSV03]. In this model, the decomposition of the data f into the cartoon part u and the texture-noise part v, $f=u+v$, is done so that u minimizes the functional

$$E_{OSV}(u) = \|u\|_{BV(\Omega)} + \lambda \|f-u\|^2_{\dot{H}^{-1}(\Omega)} = \int_\Omega |\nabla u|\, dA - \lambda \int_\Omega (f-u)\Delta^{-1}(f-u)\, dA, \qquad \lambda > 0, \tag{2.1}$$

where $\Omega \subset \mathbb{R}^2$ is a compact region of the plane where the image data is supported.

Osher-Solé-Vese model is obtained from the Meyer model,

$$E_{Meyer}(u) = \|u\|_{BV(\Omega)} + \lambda \|f-u\|_{G(\Omega)}, \qquad \lambda > 0, \tag{2.2}$$

where $\|f-u\|_G = \inf \|\boldsymbol{g}\|_{L^\infty(\Omega)}$, with infimum taken over all functions $\boldsymbol{g} \in L^\infty(\Omega, \mathbb{R}^2)$ such that $f-u = \nabla \cdot \boldsymbol{g}$. Using the Hodge theory, Osher, Solé, and Vese represent $\boldsymbol{g}$ as

$$\boldsymbol{g} = \nabla P + \boldsymbol{F},$$

where P is a scalar-valued function and $\boldsymbol{F}$ is a divergence-free vector field. They then express P as $P = \Delta^{-1}(f-u)$, and substitute $\|\boldsymbol{g}\|_{L^\infty(\Omega)}$ by

$$\|\nabla \Delta^{-1} P\|^2_{L^2(\Omega)} = \int_\Omega |\nabla \Delta^{-1} P|^2\, dA = -\int_\Omega P \Delta^{-1} P\, dA.$$

The divergence-free vector field $\boldsymbol{F}$ is neglected.

The variational derivative of functional (2.1) is given by

$$\delta_u E(u) \equiv \frac{\delta E(u)}{\delta u} = -\nabla \cdot \left(\frac{\nabla u}{|\nabla u|} \right) + 2\lambda \Delta^{-1}(f-u). \tag{2.3}$$

Osher, Solé, and Vese show that the value of the functional $E(u)$ is decreasing not only along the (anti)gradient flow

$$\dot{u} = -\delta_u E(u) = \nabla \cdot \left(\frac{\nabla u}{|\nabla u|} \right) - 2\lambda \Delta^{-1}(f-u), \tag{2.4}$$

where $\dot{u} \equiv du(t)/dt$, but also along the flow

$$\dot{u} = \Delta \delta_u E(u) = \Delta \left(-\nabla \cdot \left(\frac{\nabla u}{|\nabla u|} \right) \right) + 2\lambda (f-u). \tag{2.5}$$

Indeed, in the latter case,

$$\frac{dE(u(t))}{dt} = \int_\Omega \delta_u E(u)\dot{u}\, dA = \int_\Omega \delta_u E(u)\Delta\delta_u E(u)\, dA \tag{2.6}$$

$$= \int_{\partial\Omega} \delta_u E(u)\, \boldsymbol{n}_l \cdot \nabla\delta_u E(u)\, dl - \int_\Omega |\nabla\delta_u E(u)|^2\, dA. \tag{2.7}$$

The boundary term that appears after integration by parts vanishes if we impose appropriate boundary conditions. Since the right-hand side is negative-definite, the value of $E(u)$ is decreasing along the flow.

3 Alternative flows

The Osher-Solé-Vese model [OSV03] seems to yield a very reasonable decomposition of f into the cartoon part u and the texture-noise part v (v contains much less of the "cartoon" structure than TV model, thus leading to sharper image represented by the cartoon part u).

Let us approach the proposed algorithm from the analytical point of view. Since we assume that the original data f, the cartoon part u, and the texture-noise part v belong to L^2, we also want to have $\dot{u} \in L^2$, which does not follow from (2.5). Moreover, we would like u to belong to $BV \sim \mathcal{BV} = \dot{W}^{1,1}$, which means that f better appear in the expression for $\dot{u}$ with some smoothing factor.

To resolve this situation, we might consider the flow $\dot{u} = -\mathfrak{A}[\delta_u E(u)]$, where the operator $\mathfrak{A}$ satisfies the following properties:

1. $\mathfrak{A}$ is positive-definite (defines a positive-definite quadratic form);
2. $\mathfrak{A}$ is chosen so that $\mathfrak{A}[\delta_u E(u)] \in L^2(\Omega)$ as long as $u,\, f \in L^2(\Omega)$.

Let us check that this flow also decreases values of the functional $E(u)$:

$$\frac{dE(u(t))}{dt} = \int_\Omega \delta_u E(u)\dot{u}\, dA = -\int_\Omega \delta_u E(u)\mathfrak{A}[\delta_u E(u)]\, dA,$$

with the right-hand side being negative-definite since the operator $\mathfrak{A}$ was assumed to define a positive-definite quadratic form.

Remark 3.1. *If $\mathfrak{A}[\delta_u E(u)] \in H^s(\Omega)$ with $s > 0$, then $v \in H^s(\Omega)$ as well. That is, the flow can not carry away irregularities from f into v, leaving them in the cartoon part. Such flows seem too smooth for reasonable image decomposition.*

If $\mathfrak{A}[\delta_u E(u)] \notin L^2(\Omega)$, then the behavior of the flow is not clear; the flow is still trying to minimize the BV-norm, with $BV \subset L^2$, so even though $\dot{u}$ may no longer be in L^2, we expect that eventually the L^2-norm of u will become small. We will see that the better results are obtained when using "rough flows" that are not in L^2. The problem with such flows is that they lead to a numerical instability after certain number of steps.

Instead of functional (2.1), we will consider the functional

$$E(u) = \|u\|_{BV(\Omega)} + \lambda\|f - u\|^2_{H^{-1}(\Omega)}, \qquad \lambda > 0, \tag{3.1}$$

Figure 1: $s = 1$, $n = 5$; $\quad s = 1$, $n = 20$

where the norm in $H^{-1}(\Omega)$, which is the inhomogeneous version of $\dot{H}^{-1}(\Omega)$, is given by

$$\|f - u\|^2_{H^{-1}} = \int_\Omega (f - u)(1 - \Delta)^{-1}(f - u)\, dA.$$

The variational derivative of functional (3.1) is given by

$$\delta_u E(u) \equiv \frac{\delta E(u)}{\delta u} = -\nabla \cdot \left(\frac{\nabla u}{|\nabla u|} \right) - 2\lambda(1 - \Delta)^{-1}(f - u). \tag{3.2}$$

Our suggestion is to take $\mathfrak{A} = (1 - \Delta)^\alpha$, $\alpha \in \mathbb{R}$, considering the flow $\dot{u} = -(1 - \Delta)^\alpha \delta_u E(u)$, where we assume that the functional $E(u)$ is given by (3.1). That is, the flow is given by

$$\dot{u} = (1 - \Delta)^\alpha \left(\nabla \cdot \left(\frac{\nabla u}{|\nabla u|} \right) + 2\lambda(1 - \Delta)^{-1}(f - u) \right). \tag{3.3}$$

Example 3.1. $\alpha = -1/2$

Since $\dfrac{\nabla u}{|\nabla u|} \in L^\infty(\Omega) \subset L^2(\Omega)$ *(recall that* Ω *is compact), its divergence belongs to* $H^{-1}(\Omega)$*, while the second term in the brackets belongs to* $H^2(\Omega)$*. After applying the smoothing operator* $(1 - \Delta)^{-1/2}$*, we obtain a function from* L^2*.*

Remark 3.2. *(for the above case* $\alpha = -1/2$*)*

Let u_0 *be the minimum of functional (2.1) corresponding to the function* $f_0 \in L^2$*. Then* u_0 *is a stationary solution of flow (3.3). If we change* $f_0 \to f_1 \in L^2(\Omega)$*, then the difference between the old and new stationary points,* $u_1 - u_0$*, would also be from* $L^2(\Omega)$*. On the other hand, we compute*

$$\dot{u}|_{t=0} = \lambda(1 - \Delta)^{-3/2}(f_1 - f_0) \in H^3(\Omega).$$

The explanation to this "paradox" is that, no matter how good or bad $u(t)$ *is, a priori we only know that* $\frac{\nabla u}{|\nabla u|} \in L^\infty(\Omega) \subset L^2(\Omega)$*, so that the term* $(1 - \Delta)^{-1/2}\nabla \cdot (\nabla u/|\nabla u|) \in L^2$ *leads to* $\dot{u}(t) \in L^2$ *when* $t > 0$*.*

Remark 3.3. *(Computational trick)*

If we want to compute the evolution of $u(t)$*,* $u(0) = 0$*, along flow (3.3), we may work in the Fourier domain, only returning to the coordinate domain* Ω *when computing* $\nabla u/|\nabla u|$*:*

$$\frac{d}{dt}\hat{u} = -\frac{\xi \cdot \hat{V}(\xi)}{\sqrt{1 + \xi^2}} + \frac{2\lambda}{(1 + \xi^2)^{1+\alpha}}(\hat{f}(\xi) - \hat{u}(\xi)), \tag{3.4}$$

$$\text{where} \quad V(x) = \frac{\nabla u(x)}{|\nabla u(x)|} \quad \text{and} \quad \nabla u(x) = (i\xi\hat{u}(\xi))\check{}. \tag{3.5}$$

Remark 3.4. *Alternative approach is to introduce to flow (2.4) a regularizing factor such as the third power of* $|\nabla u|$*, getting rid of the possible singularity in the denominator, and consider the flow*

$$\dot{u} = -|\nabla u|^3 \delta_u E(u) = |\nabla u|^2 \Delta u - \nabla u \cdot \nabla(|\nabla u|^2) - 2\lambda |\nabla u|^3 \Delta^{-1}(f-u). \tag{3.6}$$

This multiplication means that the flow is "faster" at the points where the density of the total variation, $|\nabla u|$*, is larger, which seems to make physical sense. We do not have a decent analytical interpretation of this expression, since a priori we do not know to which space* $|\nabla u|$ *belongs.*

4 Independence of the second term $(f-u)$ in the OSV model

When considering the first and second terms in the equations (2.4) and (2.5), we notice that the difference in the order (say, for picture with 256×256 pixels) could be as large as $128^2 \sim 1.6 \cdot 10^6$. This means that the influence of the second term on the flow is negligible; this can be seen on Figures 2, 3.

Figure 2: [β =0-0] $\alpha, \nu, \lambda, n =$ x0.0x1000x0.1x10; $\alpha, \nu, \lambda, n =$ x0.0x1000x0.1x20

Figure 3: [β =0-0] $\alpha, \nu, \lambda, n =$ x0.0x1000x1000x10; $\alpha, \nu, \lambda, n =$ x0.0x1000x1000x20

The second parameter ν in the above pictures is introduced in front of the first term in (3.4) to have a better control in computations. (See also (5.1).)

5 How the second term can affect the flow

We suggest "equating" orders of the first and second terms in (2.4) and (2.5) in the following way:

$$\frac{d}{dt}\hat{u} = (1+\xi^2)^{\alpha} \cdot \left(\nu \cdot i\xi \cdot \hat{V}(\xi) + 2\lambda \, (1+\xi^2)^{\beta} \, (\hat{f}(\xi) - \hat{u}(\xi)) \right), \tag{5.1}$$

where $V(x)$ and $\nabla u(x)$ are from (3.5). This corresponds to considering the flow

$$\dot{u} = (1-\Delta)^{\alpha} \left(\nu \cdot \nabla \cdot \left(\frac{\nabla u}{|\nabla u|} \right) + 2\lambda (1-\Delta)^{\beta} (f-u) \right). \tag{5.2}$$

For $\beta = 1.5$, and $\alpha = 0$, then the increase in λ doesn't let the flow carry over the bulk parts, i.e. parts with slower oscillations into the $f-u$ part. On Figures 4, 5 one can see that it stabilizes the flow, removes the shiny gloss and only small oscillatory patterns get transfered into the $f-u$ part.

Figure 4: [β =1-5] $\alpha, \nu, \lambda, n =$ x0.0x1000x1x10; $\alpha, \nu, \lambda, n =$ x0.0x1000x1x20

Figure 5: [β =1-5] $\alpha, \nu, \lambda, n =$ x0.0x1000x1000x10; $\alpha, \nu, \lambda, n =$ x0.0x1000x1000x20

Similar results for $\beta = 2.0$ and $\alpha = 0.0$ are shown on Figures 6, 7.

Note that the flow which was used in the above pictures is the same as in Osher-Rudin initial model, since the power $\alpha = 0.0$.

Next we show the results when $\alpha = 0.5$ (and $\beta = 1.5$), i.e. the flow is rougher but it does not transfer any bulk of information from the cartoon part into the $f-u$ part, it only carries over the texture pattern. When comparing with above figures, one can notice (Figures 8, 9, 10) that

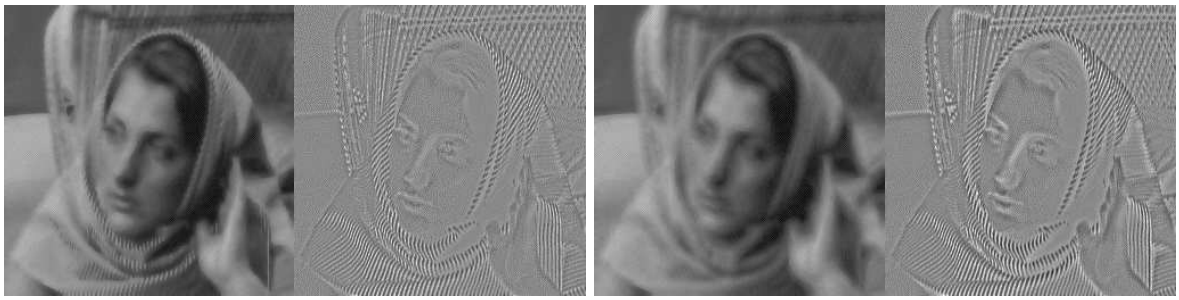

Figure 6: [β =2-0] $\alpha, \nu, \lambda, n =$ x0.0x1000x1x10; $\alpha, \nu, \lambda, n =$ x0.0x1000x1x20

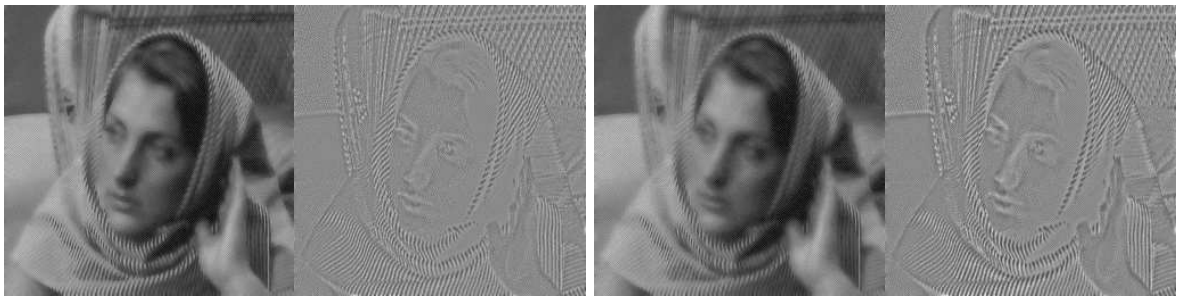

Figure 7: [β =2-0] $\alpha, \nu, \lambda, n =$ x0.0x1000x10x10; $\alpha, \nu, \lambda, n =$ x0.0x1000x10x20

there are no details from the face such as eyes, nose, etc, but only small oscillatory pattern from the woman's scarf and the background got transfered. The flow is also more stable, meaning there is no much difference in pictures between 10 iterations and 20 as there are more and more from the original picture gets transfered by the flow in all pictures above.

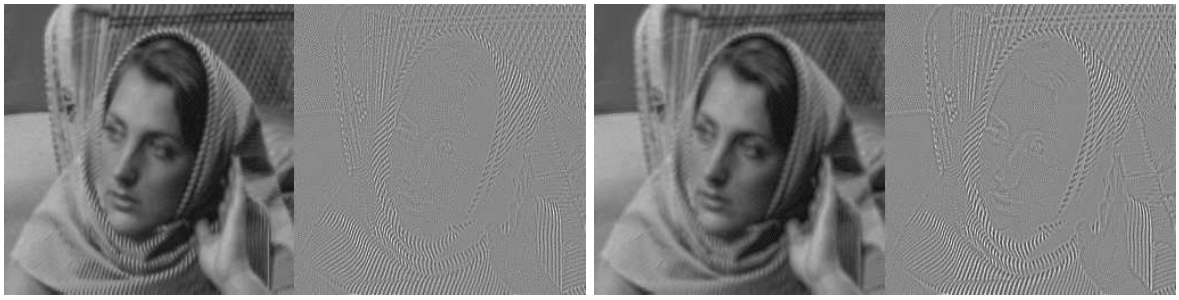

Figure 8: [β =1-5] $\alpha, \nu, \lambda, n =$ x0.5x10x0.1x10; $\alpha, \nu, \lambda, n =$ x0.5x10x0.1x20

Figure 9: [β =1-5] $\alpha, \nu, \lambda, n =$ x0.5x10x1x10; $\alpha, \nu, \lambda, n =$ x0.5x10x1x20

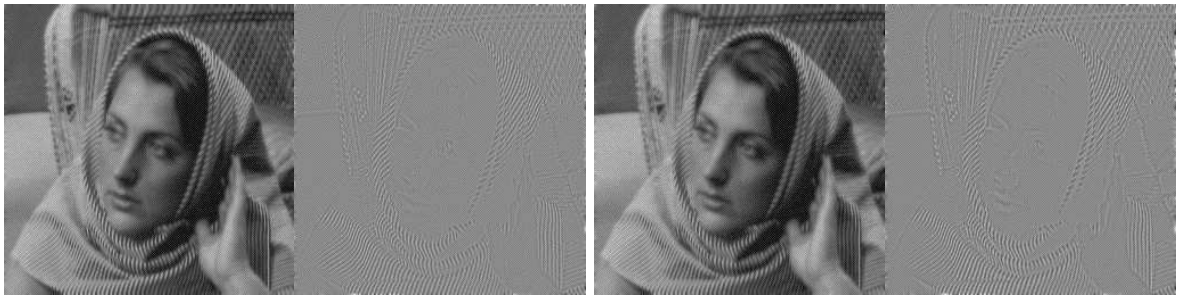

Figure 10: [β =1-5] $\alpha, \nu, \lambda, n =$ x0.5x10x10x10; $\alpha, \nu, \lambda, n =$ x0.5x10x10x20

On Figures 11, 12, 13, we see fast separation into the cartoon and texture in the case $\alpha = 1.0$ (the flow is even rougher the before). Here $\beta = 1.0$.

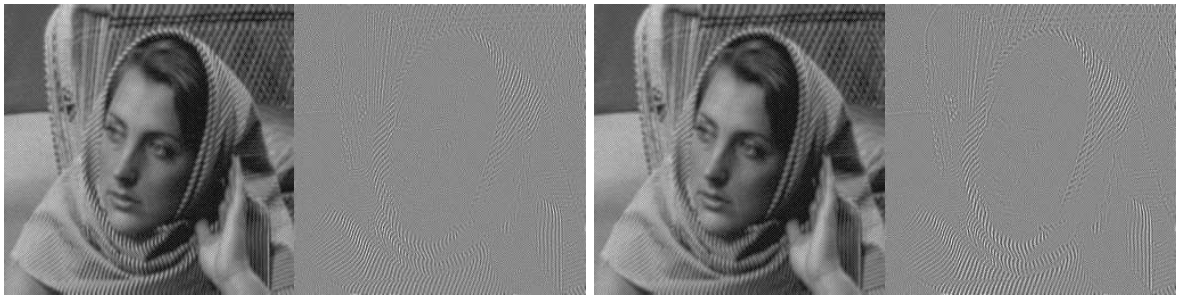

Figure 11: [β =1-0] α, ν, λ, n =x1x0.1x0.1x10; α, ν, λ, n =x1x0.1x0.1x20

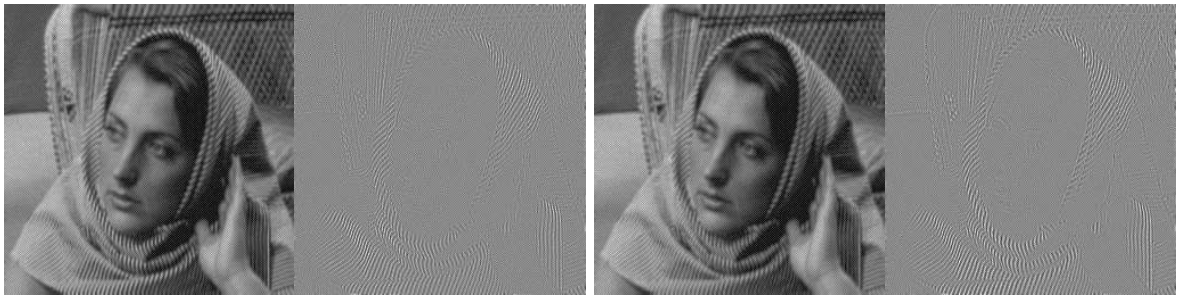

Figure 12: [β =1-0] α, ν, λ, n =x1x0.1x1x10; α, ν, λ, n =x1x0.1x1x20

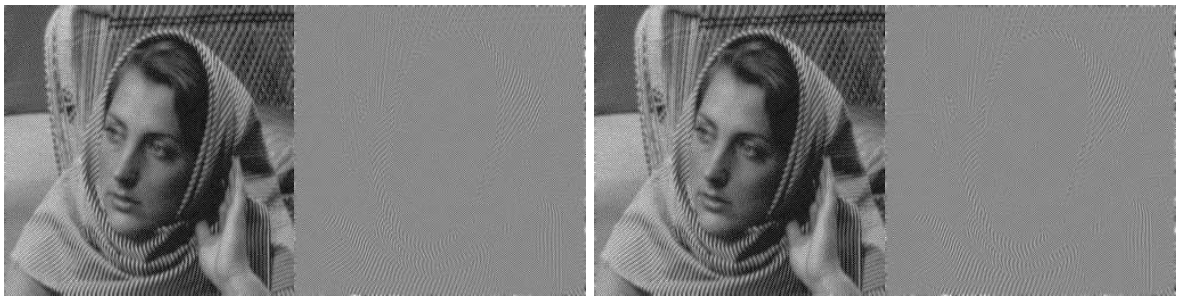

Figure 13: [β =1-0] α, ν, λ, n =x1x0.1x10x10; α, ν, λ, n =x1x0.1x10x20

ACKNOWLEDGMENTS

The author would like to thank Andrea Bertozzi for introducing her to the field of image processing. The author would like to thank Triet Li for the first version of the TV minimization code and Andrew Comech for discussions and computational help. The author is grateful to the Los Alamos National Lab for partial funding of this project.

References

[D92] Ingrid Daubechies, *Ten lectures on wavelets*, CBMS-NSF Regional Conf. Series in Appl. Math., 61, (SIAM), Philadelphia, PA, 1992. xx+357 pp.

[DL92] Ron DeVore and B. Lucier, *Fast wavelet techniques for near optimal image compression algorithms*, IEEE Military Communications Conference, October 11-14 (1992).

[DJ94] David L. Donoho and I. M. Johnstone, *Ideal spatial adaptation by wavelet shrinkage*, Biometrika **81** (1994), no. 3, 425–455.

[DJKP96] David L. Donoho, I. M. Johnstone, Gérard Kerkyacharian, and Dominique Picard, *Density estimation by wavelet thresholding*, Ann. Statist. **24** (1996), no. 2, 508–539.

[DJKP97] D. L. Donoho, I. M. Johnstone, G. Kerkyacharian, and D. Picard, *Universal near minimaxity of wavelet shrinkage*, Festschrift for Lucien Le Cam, Springer, New York, 1997, pp. 183–218.

[Mey01] Yves Meyer, *Oscillatory patterns in image processing and nonlinear evolution equations*, University Lecture Series, vol. 22, American Mathematical Society, Providence, 2001.

[MS85] David Mumford and J. Shah, *Boundary detection by minimizing functionals*, Proc. IEEE Conf. Comp. Vis. Pattern Recognition, 1985.

[OSV03] Stanley Osher, Andrés Solé, and Luminita Vese, *Image decomposition and restoration using total variation minimization and the H^{-1} norm*, Multiscale Model. Simul. **1** (2003), no. 3, 349–370 (electronic).

[RO94] Leonid Rudin and Stanley Osher, *Total variation based image restoration with free local constraints*, Proceedings of the IEEE ICIP, Austin, USA **1** (1994), 31–35.

[ROF92] Leonid Rudin, Stanley Osher, and E. Fatemi, *Nonlinear total variation based noise removal algorithms*, Physica D, **60** (1992), 259–268.

[VO03] Luminita Vese and Stanley Osher, *Modeling textures with total variation minimization and oscillating patterns in image processing*, J. Scientific Comput. **9** (2003), 553–572.

Department of Mathematics, Duke University, Durham, NC 27708

svetlana@math.duke.edu